Catal Lett (2012) 142:854–859
DOI 10.1007/s10562-012-0836-y

'Ship-in-a-Bottle' Synthesis of MoS_2/MCM-41 Catalysts by Decomposition of Single Source Precursor in Mesoporous Channel

Hongfei Fan · Xin Jin · Lei Wang · Christopher T. Williams · Tianxi Cai · Changhai Liang

Received: 18 February 2012 / Accepted: 24 April 2012 / Published online: 15 May 2012

Abstract MoS_2/MCM-41 catalysts have been prepared by thermal decomposition of MCM-41 with cetyltrimethylammonium thiomolybdate, which was synthesized by reaction between ammonium thiomolybdate and cetyltrimethylammonium bromide left in the pore channel of MCM-41. The obtained catalysts exhibit type IV adsorption–desorption isotherms, indicating that MCM-41 mesoporous structure is retained during the synthesis process. With increasing loading of MoS_2, the catalytic activity of MoS_2/MCM-41 for HDS of DBT first increases, followed by a leveling off above 10 % MoS_2 loading, likely due to lack of accessibility to additional active sites. For the first time over MoS_2 catalysts, the DDS (i.e., hydrogenolysis) reaction pathway is favored with 100 % selectivity. This unique performance is associated with single layer MoS_2 sites stabilized within the pores of the MCM-41 support.

Keywords Ship-in-a-bottle · Molybdenum sulfide · Mesoporous material · Hydrodesulfurization

1 Introduction

Molybdenum disulfide (MoS_2) has been the subject of significant research for applications including for catalytic hydrodesulfurization (HDS) and hydrodenitrogenation (HDN) of petroleum [1], as an additive for lubricating oil [2–4], and in non-aqueous lithium batteries [5]. Since World War II, MoS_2 have been the basis for some of the most widely used hydrocarbon processing catalysts [6]. Conventional catalysts include mainly Mo- or W-based catalysts supported by γ-Al_2O_3 [7], which are active in converting thiophene and benzothiophene, but not efficient enough to desulfurize the most refractory sulfur-containing polyaromatic compounds, such as dibenzothiophene (DBT) and its alkyl-substituted derivatives. In addition to Al_2O_3, various materials such as SiO_2, TiO_2 [2, 3], ZrO_2 [4, 5], MgO [6], zeolites [7], and clays have been experimentally used as supports in order to improve their catalytic properties.

In the last decade, MoS_2 supported on mesoporous materials and unsupported MoS_2 have been synthesized in order to improve catalytic activity toward large heterocyclic organic molecules [8–10]. Corma et al. [11] used Al-MCM-41 to support Ni–Mo catalysts for application in hydrocracking of vacuum gas oil, and found that Al-MCM-41-supported catalysts were more active in HDS, HDN, and hydrocracking than those supported over USY or γ-Al_2O_3. Wang et al. [12] prepared Co–Mo/MCM-41 catalysts for deep HDS, and found that sulfur atom exchange between sulfur-containing molecules and the active sites is involved in the HDS reaction. Accordingly, a reaction mechanism for HDS was proposed, which is in accordance with the isotope tracer results, the rim-edge model [13], and DFT calculations [14–16].

In the case of HDS catalysts, the metal-support linkages are seen to play an important role. The catalysts with higher tendency to form such linkages are known as "Type-I catalysts," while the absence of such linkages leads to "Type-II catalysts". Since these chemical linkages inhibit the mobility of the MoS_2 particles on the support surface, the intrinsic activity of Type-I structures are expected to be lower than

H. Fan · X. Jin · L. Wang · T. Cai · C. Liang (✉)
Laboratory of Advanced Materials and Catalytic Engineering, School of Chemical Engineering, Dalian University of Technology, Dalian 116024, China
e-mail: changhai@dlut.edu.cn
URL: http://finechem.dlut.edu.cn/liangchanghai/

C. T. Williams
Department of Chemical Engineering, University of South Carolina, Columbia, SC 29208, USA

Type-II structures [17]. Conventional supported MoS_2 catalysts are mainly prepared by impregnating with molybdate precursors solution, followed by calcination and then sulfidization in situ or ex situ under H_2S or sulfur-containing compounds and H_2 [12, 18, 19]. Supported MoS_2 catalysts can also be obtained directly through thermal decomposition of supported thiomolybdates in inert atmosphere [20–22]. In this paper, we prepared a novel MoS_2 catalyst supported on the MCM-41. Cetyltrimethylammonium bromide (CTAB), which was used as a template in the synthesis of MCM-41, was reacted with ammonium thiomolybdate (ATM, $(NH_4)_2MoS_4$) according to the Eq. (1).

$$(NH_4)_2MoS_4 + 2(C_{16}H_{33})N(CH_3)_3Br \rightarrow \left[(C_{16}H_{33})N(CH_3)_3\right]_2MoS_4 + 2NH_4Br \quad (1)$$

The formed cetyltrimethylammonium thiomolybdate (CTMATM) was located in the mesoporous channel of MCM-41. This route is essentially a "ship-in-a-bottle" method [23–25]. Thermal decomposition of this tetraalkylammonium thiosalt precursor, which was consistent with the Eq. (2), directly led to formation of MoS_2 in the mesoporous channel of MCM-41.

$$\left[(C_{16}H_{33})N(CH_3)_3\right]_2MoS_4 \rightarrow 2(C_{16}H_{33})N(CH_3)_2 + (CH_3)_2S_2 + MoS_2 \quad (2)$$

2 Experimental

2.1 Catalyst Preparation

ATM was synthesized according to the method described in Ref. [26, 27]. The "ship-in-a-bottle" synthesis was carried out at room temperature in two steps: first, a certain amount of the precursor ATM was dissolved in 5 ml formamide, followed by addition of 0.50 g MCM-41 with CTAB. After 2 h stirring, the products were filtered without washing and dried under vacuum over night at 353 K. Finally the dried sample CTMATM/MCM-41 was decomposed to obtain MoS_2/MCM-41 under flowing argon, heating from room temperature to 673 K at a rate of 10 K min^{-1} and kept at that temperature for 1 h. MoS_2/MCM-41 with 5, 10, 15 and 20 wt% MoS_2 loadings were prepared under above-mentioned conditions. MoS_2(U) was prepared by direct decomposition of ATM using the showing decomposition procedure. MoS_2(E) was obtained by etching the MCM-41 of 10 wt% MoS_2 loading sample using sodium hydroxide aqueous solution (pH = 11).

2.2 Catalyst Characterization

Fourier transform infrared (FTIR) spectra were collected at room temperature on Nicolet Impact 410 with a resolution of 4 cm^{-1}. Nitrogen adsorption and desorption isotherms at 77 K were measured using Micromertics 2010. The specific surface areas of samples were calculated by BET (Brunauer–Emmett–Teller) method and pore volumes were calculated from the volume of liquid nitrogen at $p/p_0 = 0.98$. X-ray diffraction (XRD) analysis of the samples was carried out using a Rigaku D/Max-RB diffractometer with Cu Kα monochromatized radiation source ($\lambda = 1.54178$ Å), operated at 40 kV and 100 mA. The morphology and distribution of as-prepared samples were studied by transmission electron microscopy (TEM, Philips CM200 FEG) equipped with energy dispersive X-ray spectroscopy (EDS), operated at 200 kV. Element analysis was performed on Elementar VarioEL III and inductively coupled plasma atomic emission spectroscopy (ICP-AES) (Perkin-Elmer Optima 2000DV).

2.3 Catalyst Test

The HDS of DBT was carried out in a continuous fixed-bed reactor at 613 K and 3.0 MPa. Passivated catalysts (0.05 g with particle size 2.5 ± 0.3 mm) were activated in situ with H_2 at 3 MPa and 623 K for 1 h. The liquid reactant was composed of 2.0 wt% DBT reactant, 0.3 wt% decane (as internal standard for gas chromatography (GC) analysis), 97.7 wt% decalin (as solvent). Liquid samples were analyzed by an off-line gas chromatography (GC 7890F) equipped with a flame ionization detector and a SE-54/52 capillary column.

3 Results and Discussion

3.1 "Ship-in-a-Bottle" Synthesis

Since ATM was used to react with the CTAB in the MCM-41 to synthesize CTMATM directly, different products were synthesized in the channel of MCM-41 in every experimental stage. Thus, FTIR spectroscopy was used to characterize the different functional groups at every stage of synthesis. In the FTIR spectra in Fig. 1, the peak in the region 3,400 cm^{-1} is due to OH vibrational modes arising from water residues in the samples. The CTAB/MCM-41, CTMATM and CTMATM/MCM-41 all have two characteristic peaks at 2,926 and 2,850 cm^{-1}, assigned to the asymmetric and symmetric CH_2 stretching modes, and peaks in the 1,450–1,500 cm^{-1} region have been assigned to CH_2 scissoring and CH_3–(N^+) asymmetric bending modes [28]. These results prove presence of $CTMA^+$ functional group in these samples, and the alkane characteristic of samples retains during the reaction process. The peaks at 1,230 and 1,075 cm^{-1} are due to the Si–O–Si

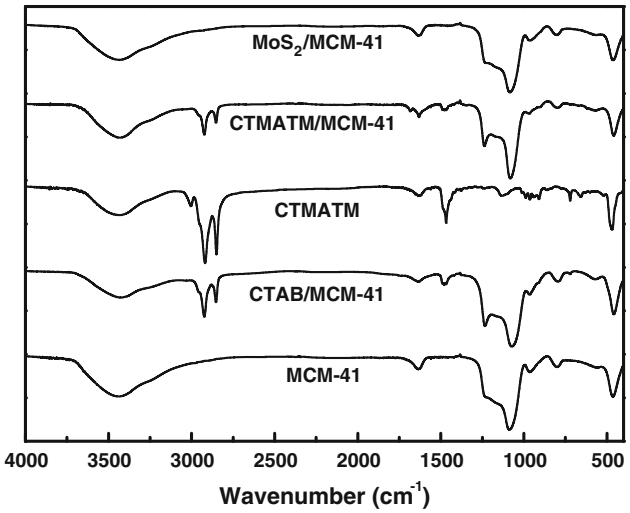

Fig. 1 FTIR spectra of MCM-41, CTAB/MCM-41, CTMATM, CTMATM/MCM-41 and MoS_2/MCM-41

vibrational modes [28], which reveal that the MoS_2/MCM-41 keeps the structure of MCM-41.

3.2 XRD

XRD patterns of the MoS_2/MCM-41 with different MoS_2 loading are shown in Fig. 2a. An increase of MoS_2 loading led to the formation of poorly crystalline MoS_2 characterized by diffraction peaks at 33°, 40°, and 58°. The broad peak at about 22° is caused by the amorphous MCM-41 silica. Interestingly, compared with unsupported sulfide prepared from thermal decomposition of ATM (MoS_2(U)), the MoS_2(E) and MoS_2/MCM-41 samples are missing the (002) reflection at 14°. This suggests that the layered structure of MoS_2 is destroyed and that the formed MoS_2 on the support may be single-layered [6]. Small-angle XRD patterns of MoS_2/MCM-41 with different MoS_2 loadings were acquired (Fig. 2b). Three characteristic reflections (100), (110), and (200) of hexagonal mesoporous MCM-41 (space group *p6mm*) are observed for all samples, providing strong evidence that the primary structure of MCM-41 consisting of well-ordered channels is preserved after the incorporation of MoS_2. The decrease of the peak intensity may be caused by phase cancellation between the pore walls and the guest species, strong absorption of X-rays by MoS_2 and/or partial loss of the higher order of the mesoporous structure. This well-known phenomenon has been described previously in the literature [20, 21, 29].

3.3 Nitrogen Physisorption

As shown in Fig. 3, all materials also show type IV isotherms that are typical characteristics of mesoporous materials. This observation further demonstrates that the

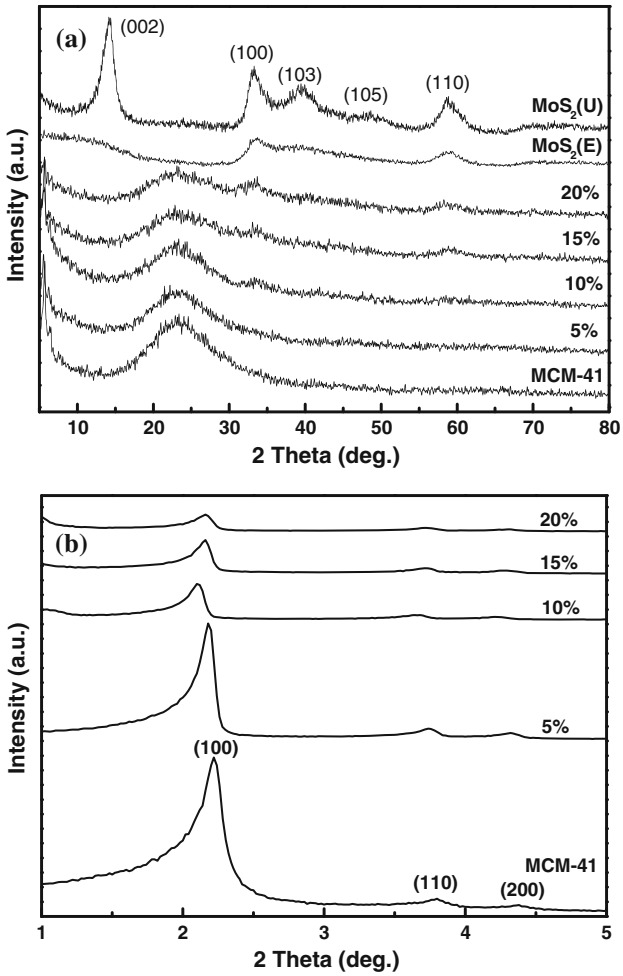

Fig. 2 Wide-angle (**a**) and small-angle (**b**) XRD patterns of MoS_2/MCM-41 with different MoS_2 loadings

incorporation of CTAB and ATM species does not destroy the mesoporous structure of MCM-41. Table 1 summarizes the element content, BET surface areas and pore volumes of different samples. Generally, the specific surface area decreases after MoS_2 loading. Below 10 % MoS_2/MCM-41 sample, the specific surface area and the pore volume of the samples increase with increasing MoS_2 loading, which results from the thermal decomposition of CTMATM in the pore. Above 10 % MoS_2/MCM-41 sample, the specific surface area and the pore volume decrease with increasing MoS_2 loading, mainly due to both the dilution of the support and pore blocking by MoS_2, which show obvious effects on the structure parameters of MoS_2/MCM-41 samples. However, the nitrogen adsorption–desorption isotherms from $p/p_0 = 0$ to 0.35 suggest that there exist micropores in these materials, which may be due to the coke from decomposition of CTMATM under nitrogen atmosphere. The around 7.0 wt% C content in the calcined MoS_2/MCM-41 samples confirms the existence of coke. Thus, the sample with 10 % MoS_2 loading has higher BET

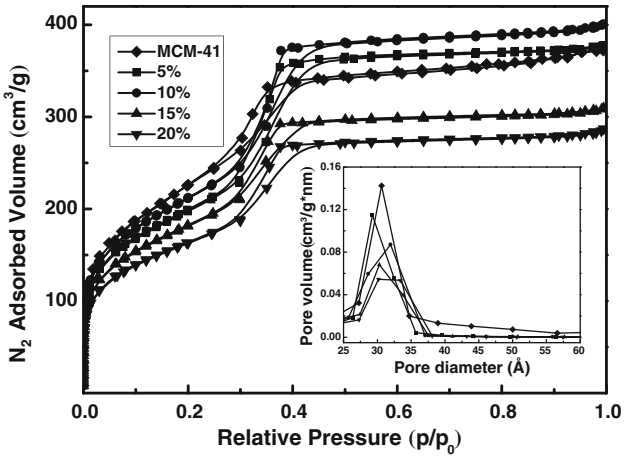

Fig. 3 N_2 adsorption–desorption isotherms and pore-size distributions (*inset*) of MoS_2/MCM-41 with different MoS_2 loading

surface area than that with 5 % loading. While the pore diameters of 5, 10, 15 and 20 % MoS_2/MCM-41 are all in the range of 2.5–3.8 nm as shown in Fig. 3 Inset. The Mo/S atomic ratio is around 0.5 calculated from the element analysis, which indicates that MoS_2 is formed in the pores of MCM-41 indirectly.

3.4 TEM

Typical TEM images of the 10 % MoS_2/MCM-41 with side view (Fig. 4a) and front view (Fig. 4b) to the pore axis indicate that the mesoporous structure of MCM-41 is still kept and MoS_2 particles are not evenly distributed in the mesoporous channels of the MCM-41. This is consistent with the XRD and N_2 adsorption results discussed above. However, the EDS spectrum (Fig. 4c) confirms the existence of Mo and S in identical atomic ratios to the nominal bulk values. This provides indirect proof that MoS_2 particles are in the MCM-41.

3.5 Catalytic Activity

Figure 5 shows the conversion and selectivity obtained over the MoS_2/MCM-41 catalysts. All the MoS_2/MCM-41 catalysts favor the direct desulfurization (DDS) pathway (i.e., C–S bond hydrogenolysis) with 100 % selectivity. This is the first such observation for Mo-based catalysts, and is attributed to the single layer MoS_2 sites stabilized by the MCM-41 pore structure. The 10 % MoS_2/MCM-41 sample has the highest conversion of DBT (23 %), although the other higher loading samples are similar. This result suggests that at higher loadings the effectiveness of any additional active sites is limited by either structural or mass transfer effects.

4 Conclusions

In summary, MoS_2/MCM-41 catalysts were prepared by thermal decomposition of CTMATM/MCM-41 obtained by the "ship-in-a-bottle" method. The obtained catalysts exhibit type IV adsorption–desorption isotherms, indicating that the MCM-41 mesoporous structure is retained during the synthesis process. With increasing loading of MoS_2, the catalytic activity of MoS_2/MCM-41 for HDS of DBT first increases, followed by a leveling off above 10 % MoS_2 loading, likely due to lack of accessability to additional active sites. For the first time over MoS_2 catalysts, the DDS (i.e., hydrogenolysis) reaction pathway is favored with 100 % selectivity. This unique performance is associated with single layer MoS_2 sites stabilized within the pores of the MCM-41 support.

Table 1 Element content, BET surface area and pore volume of MoS_2/MCM-41 samples with different MoS_2 loadings

Sample (before/after)	Element content (wt%)				S_{BET}[a] (m^2/g)	V (cm^3/g)
	C[b]	N	S	Mo[c]		
MCM-41	34.5/–	2.0/–	–	–	822	0.60
5 %	32.8/6.8	2.2/0.1	1.9/1.8	1.5/2.7	714	0.65
10 %	31.5/7.4	2.7/0.1	3.6/3.5	2.5/5.5	765	0.69
15 %	30.4/7.8	3.1/0.2	5.9/5.5	4.6/9.0	655	0.56
20 %	29.1/8.3	3.5/0.2	7.7/7.1	5.7/11.2	582	0.51

Element content was analyzed from the samples before and after calcination

[a] Specific surface area (S_{BET}) and pore volume (V) were calculated from nitrogen physisorption on the calcined samples

[b] C, N, S element content were analyzed by elemental analyzer

[c] Analyzed by ICP-AES

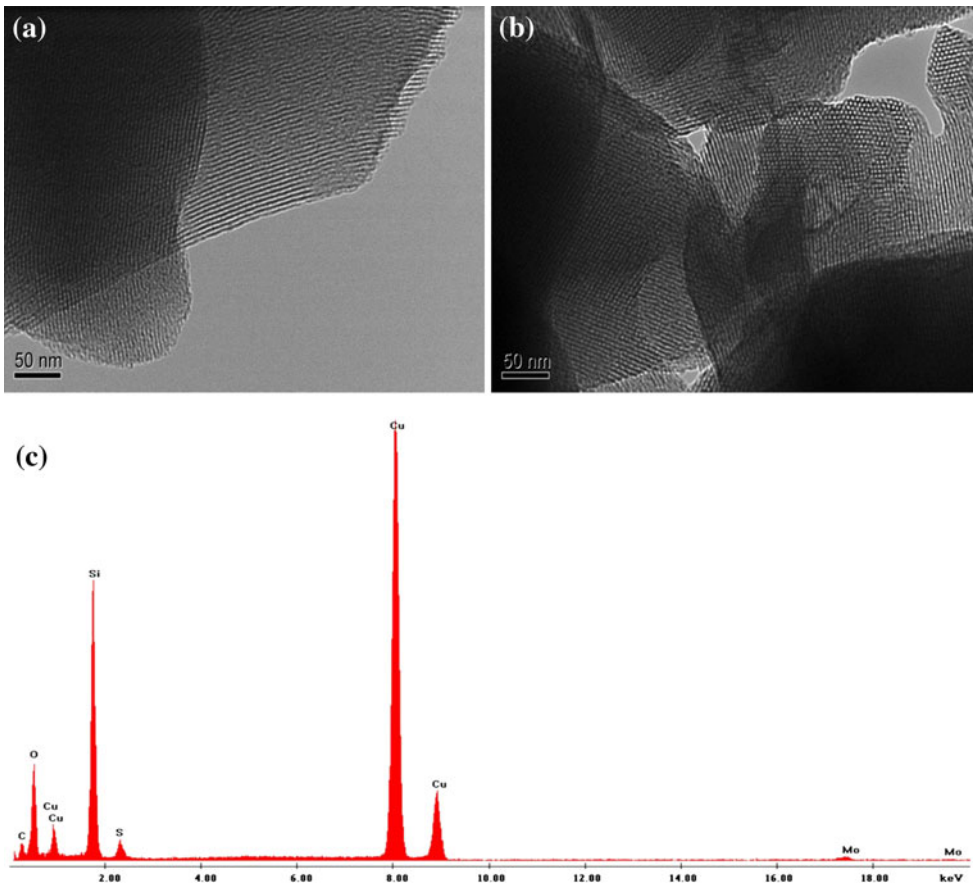

Fig. 4 Representative TEM images (**a**, **b**) and EDS spectrum (**c**) of 10 % MoS_2/MCM-41. For **a** side view to the pore axis, and **b** front view to the pore axis

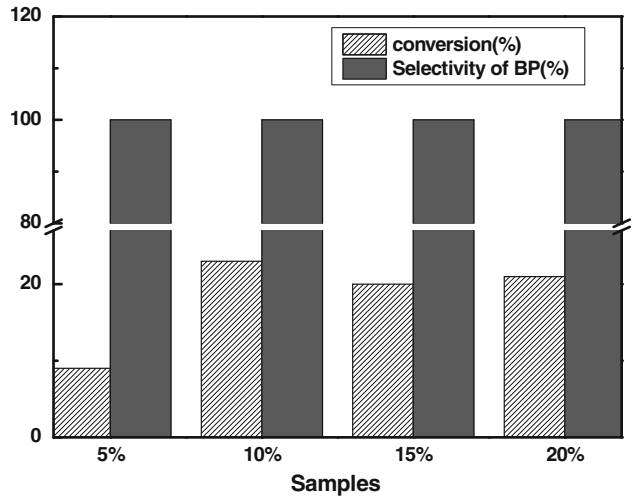

Fig. 5 Catalytic performance of MoS_2/MCM-41 with different MoS_2 loadings for HDS of DBT

Acknowledgments We gratefully acknowledge the financial support provided by the National Natural Science Foundation of China (No. 20973029) and the Fundamental Research Funds for the Central Universities (DUT12YQ03).

References

1. Thakur DS, Delmon B (1985) J Catal 91:308
2. Ogilvy JA (1993) Wear 160:171
3. Fusaro RL (1982) ASLE Trans 25:141
4. Winer WO (1967) Wear 10:422
5. Whittingham MS (1976) Science 192:1126
6. Chianelli RR, Prestridge EB, Pecoraro TA, Deneufville JP (1979) Science 203:1105
7. Yoshimura Y, Matsubayashi N, Sato T, Shimada H, Nishijima A (1991) Appl Catal A Gen 79:145
8. Jaramillo TF, Jorgensen KP, Bonde J, Nielsen JH, Horch S, Chorkendorff I (2007) Science 317:100
9. Schweiger H, Raybaud P, Kresse G, Toulhoat H (2002) J Catal 207:76
10. Tenne R (2006) Nat Nanotechnol 1:103
11. Corma A, Martinez A, Martinezsoria V, Monton JB (1995) J Catal 153:25
12. Wang A, Wang Y, Kabe T, Chen Y, Ishihara A, Qian W (2001) J Catal 199:19
13. Daage M, Chianelli RR (1994) J Catal 149:414
14. Byskov LS, Norskov JK, Clausen BS, Topsoe H (1999) J Catal 187:109
15. Knudsen KG, Cooper BH, Topsoe H (1999) Appl Catal A Gen 189:205
16. Topsoe H, Knudsen KG, Byskov LS, Norskov JK, Clausen BS (1999) Stud Surf Sci Catal 121:13
17. Joshi YV, Ghosh P, Daage M, Delgass WN (2008) J Catal 257:71
18. Gutiérrez OY, Pérez F, Fuentes GA, Bokhimi X, Klimova T (2008) Catal Today 130:292
19. Krishnamurthy S, Panvelker S, Shah YT (1981) AlChE J 27:994
20. Huang ZD, Bensch W, Kienle L, Fuentes S, Alonso G, Ornelas C (2008) Catal Lett 124:24
21. Huang ZD, Bensch W, Kienle L, Fuentes S, Alonso G, Ornelas C (2008) Catal Lett 122:57

22. Rivera-Munos ER, Lardizabal D, Alonso G, Aguilar A, Siadati MH, Chianelli RR (2003) Catal Lett 85:147
23. Herron N (1986) Inorg Chem 25:4714
24. Diegruber H, Plath PJ, Schulzekloff G, Mohl M (1984) J Mol Catal 24:115
25. Meyer G, Wohrle D, Mohl M, Schulzekloff G (1984) Zeolites 4:30
26. Jin X, Ma CL, Yi YJ, Zhang QM, Qiu JS, Liang CH (2010) J Phys Chem Solids 71:642
27. Berhault G, Mehta A, Pavel AC, Yang JZ, Rendon L, Yacaman MJ, Araiza LC, Moller AD, Chianelli RR (2001) J Catal 198:9
28. Holmes SM, Zholobenko VL, Thursfield A, Plaisted RJ, Cundy CS, Dwyer J (1998) J Chem Soc Faraday Trans 94:2025
29. Carrado KA, Kim JH, Song CS, Castagnola N, Marshall CL, Schwartz MM (2006) Catal Today 116:478